# MRI evidence for a “Coffee-front effect” in drying porous media

E. Keita, P. Faure, S. Rodts, P. Coussot

*Université Paris-Est, Laboratoire Navier (UMR8205), ENPC-IFSTTAR-CNRS, 2 Allée Kepler, Champs sur Marne, France*

**Abstract:** After drying colloidal particles suspended in a porous medium a concentration gradient appears. Using $^{1}$H MRI we propose a new protocol to observe simultaneously the distributions of air, liquid and colloid through the unsaturated solid porous structure. Thus we show that the above phenomenon comes from a *receding-front effect*: the elements migrate towards the free surface of the sample and accumulate in the remaining liquid films. Our understanding of the process makes it possible to establish a simple model without diffusion predicting the drying rate and the concentration distribution in time in excellent agreement with the experimental observations.

## 1. Introduction

After drying a coffee suspension initially homogeneously dispersed in a porous medium (white glass bead packing) a surprising concentration gradient appears (see Fig.1). The initially black sample (see Figure 1a) has finally shaded tones with darker regions around the sample free surface and white regions almost free of particles around the bottom (see Figure 1b). Thus coffee particles have moved from the bottom to the upper layers during the drying process, which suggests that they are transported with the liquid towards the free surface.

Such a situation in which a porous medium filled with a suspension dries is extremely frequent in industry and nature. It plays a major role in the colloid-facilitated transport of pollutants through soils [1], salt crystallization leading to deterioration of building materials [2], clogging of road surfaces [3], and evolutions of soil fertility and workability [4]. However, as far as we know, whereas the behavior of ion solutions in drying porous media has been fairly investigated, there is no straightforward observation and quantification of the colloid dynamics under such conditions and the phenomenon described above has not been mentioned.

Colloidal particles dynamics in drying droplets has been widely explored. In particular it has been shown that a coffee-ring effect occurs as a result of particle accumulation towards the contact line [5]. The corresponding dry front progression has been directly observed in thick films of colloidal suspension [6] and through deposits of dye at the drying spots in porous media [7]. Further studies showed how this effect may be suppressed, mainly through Marangoni flows (temperature, solvent mixture) [8], or more surprisingly by changing the particle shape [9]. Besides it was shown that at high concentration a solid phase forms that can buckle or crack due to high capillary stresses [10-13], and that advection-diffusion models predict well the colloid accumulation in liquid droplets [14] or salt solution in porous media [2].

One knows that simple liquid evaporates from porous medium through a succession of regimes [15-16] including mainly a first stage of liquid redistribution via capillary effects (constant rate period) [17] and a second stage of dry front penetration (falling rate period). The impact of the presence of solid additives in the liquid has not been taken into account, in particular due to the difficulty to obtain accurate measurements of the evolution of the colloidal phase inside the porous medium. MRI is a powerful tool to look into opaque materials which has been used to measure either the water distribution or phase changes inside porous media [2, 18-19] or the solid concentration in colloidal systems [20]. However, the usual unique MRI signal cannot account for the multiphasic nature of a colloidal system in a porous medium. In this letter, we study such systems with a new MRI protocol to observe at the same time the distribution or air, liquid and colloid through the unsaturated solid porous structure. We show that the drying process relies on a new general phenomenon: a *receding coffee-front effect.* The elements migrate towards the free surface of the sample and accumulate in the remaining liquid films, which leads to a continuous decrease in concentration from the top to the bottom of the sample at the end of drying. Our understanding of the process makes it possible to establish a simple model predicting the drying rate and the concentration distribution.

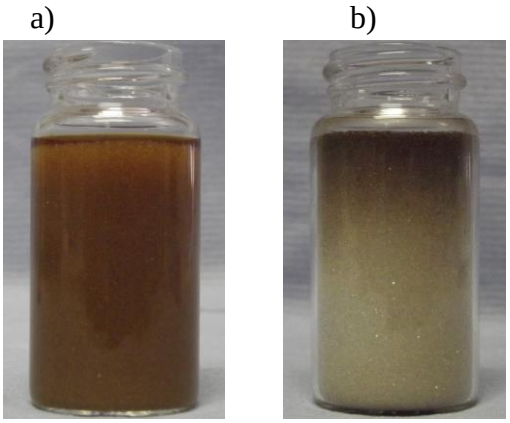


FIG. 1. (Color online) Porous medium made of 257 (+/- 9) µm sodiocalcic glass beads packing (from *CVP Abrasif & Broyage*, cleaned with NaOH and deionized water, volume fraction: 60.3%) homogeneously filled with a coffee suspension (3.5% weight in water) before (a, beads, water, coffee) and after (b, beads, coffee) drying under natural room convection and ambient temperature.

## 2. Experiments

Beyond the first illustration above it is critical to observe the physical processes inside the sample, in particular the liquid and particle motions. In that aim, instead of coffee we used hydrophilic colloidal silica nanoparticles (Ludox HS-40 diameter: 20 nm, density ~ 2.45)

suspended in water (pH = 9.8 to maintain the particle electrostatic repulsion) at initial volume fractions ($\psi_0$) ranging from 0 to 15%, and we carried out tests with the same beads (packed by hand) in a cylindrical sample under stream of dehydrated air (relative humidity < 1%) at ambient temperature ($23\,°\mathrm{C} \pm 1$) along the top surface. Their small size prevented the particles from settling. While the water evaporates we follow the local water saturation in the porous medium ($\phi$) (ratio of the water volume to the available pore volume, i.e. the void between the beads) and the volume fraction of colloids in the pores $\chi$. We can then compute the local volume fraction of colloidal particles in the liquid (water + particles) phase: $\psi = \chi/(\chi + \phi)$.

In that aim the distribution of apparent water along the sample axis was measured by a 0.5 T $^1$H MRI spectrometer with a one-dimensional double spin-echo sequence (two first echoes of the so-called Carr-Purcell-Meibom-Gill sequence [21-22] with exponential extrapolation to compensate spin-spin relaxation). Each measured value of this distribution thus corresponds to the total amount of water in a thin cross-sectional layer situated at a given position along the sample axis. The determination of local particle concentrations relies on local measurements of water spin-lattice relaxation time T1 using a conventional series of T1-weighted spin-echo profiles. As compared with free water (which from our MRI system has a relaxation time $T_{1,bulk}$=2.5s), relaxation in our samples is enhanced due to contacts with beads and particles. Provided molecular exploration of the porous network owing to Brownian motion is faster than local relaxation processes -in the spirit of the so-called 'fast exchange regime' [23-24]- the observed relaxation rate $R = 1/T_1$ is the sum of individual contributions from bulk relaxation process, water-bead and water-particle contact relaxations. Independent experiments (not shown here) indicated that the particle-water contribution varies fairly linearly over a wide range of particle/water concentrations, as in the case of clay [25] and cement [26] suspensions. Since -provided water thickness exceeds few molecular layers- relaxation at chemically homogeneous solid surfaces is reliably [27] described as $R_{surface} = \rho S/V$ where $S$ is the contact surface area between solid and liquid phases, $V$ the fluid volume, and $\rho$ the so-called surface relaxivity taken as a physical constant for a given temperature and magnetic field, we can finally write the relaxation rate in our unsaturated porous system as

$$\frac{1}{T_1} \approx \frac{1}{T_{1,bulk}} + \frac{\rho s}{\phi} + \alpha \frac{\chi}{\phi} \qquad (1)$$

$s$ is the wetted surface area to pore volume ratio, and is supposed to depend on the local saturation state and particle concentration: $s = s(\phi, \chi)$. $\alpha$ is the calibration constant of the particle contribution, and is determined from independent tests. Finally the estimation of $\chi$ from the values of $\phi$ and $T_1$ just requires a good estimation of $\rho s$. Assuming that, due to strong capillary effects, details of the fluid repartition at the pore scale –and particularly the wetted interface- mainly depend on the fluid volume, but not so much on the fluid composition, we approximate $s$ as a function $s(\phi + \chi)$. Surface terms can then be calibrated by means of independent experiments where $\chi$ is set to zero, i.e. drying experiments performed on glass bead packing initially saturated with pure water, without particles.

Previous MRI studies already reported the use of $^{1}H$ relaxation to determine local concentration of particles on colloidal systems [25, 28], even when colloidal particles are not in the situation to produce their own detectable MRI signal. Here, we propose a route to explicitly take into account the influence of the porous matrix in the relaxation process, so as to extend the approach to the more complex *simultaneous assessment* of water and colloid in a porous medium in *unsaturated* conditions (i.e. when each voxel in the picture possibly contains beads, colloids, water and air).

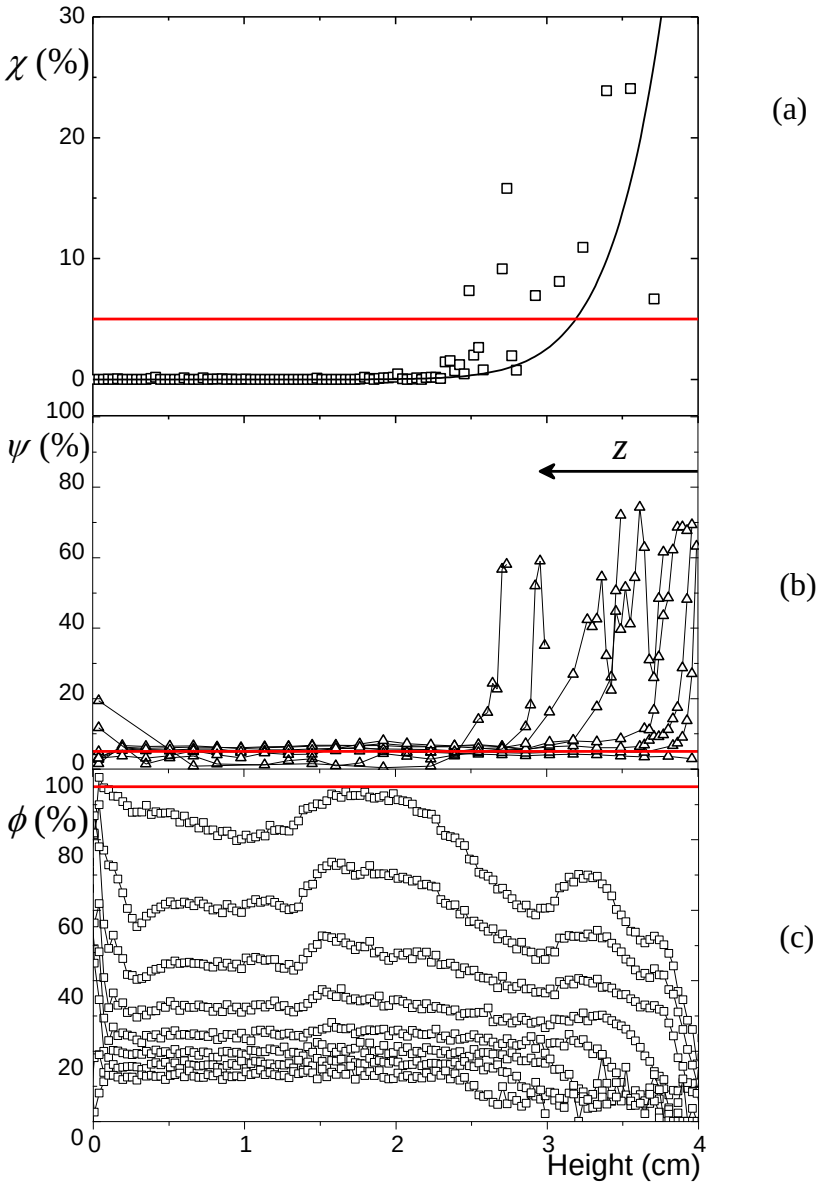


FIG. 2. (Color online) Drying through the upper free surface of a cylindrical (height = 4 cm) porous medium made of glass beads (62% volume fraction) initially filled with a colloidal suspension at 5% volume fraction in water. Drying occurs through the upper surface (right) with a steady dried air flow at 0.1 m/s leading to an initial drying rate of $1.1 \times 10^{-10}$ $m^3/s$ which corresponds to a drying velocity (see text) of $1.2 \times 10^{-7}$ m/s. MRI measurements were carried out every two hours over 4 days giving us access to: (a) the

distribution of particles in the pores at the end of the experiment (the black line corresponds to equation (4) (see text)), (b) the distribution of colloids in the liquid phase and (c) the distribution of water as a function of sample height. For the two last figures the profiles displayed are separated by 10 hours. Red thick lines represent the initial state.

Let us now look at the distribution of colloidal particles in the sample. Although it was initially homogeneous, at the end of the drying the distribution is strongly heterogeneous (see Figure 2a): despite the data scattering we clearly see that the concentration is around zero over some significant thickness then increases and reaches a value much larger than the initial one around the free surface of the sample. Such a distribution is qualitatively similar to the apparent one for the sample filled with coffee.

## 3. Discussion

These data suggest that the effect observed for the coffee in the bead packing is general: the colloidal particles tend to move towards the free surface of the sample. Finally there is a kind of coffee ring effect in a porous medium but here the colloidal particles do not accumulate essentially at the edge of the sample, they are dispersed throughout some part of the sample.

Such a result is unexpected if we think of drying in a porous medium as occurring in the form of a dry front receding through the sample. In that case water evaporation would take place all along this path and the particles would accumulate evenly along this progression. Although for salt solutions diffusion can play a significant role [2], this is not the case here with nanoparticles since the Peclet number (i.e. $V/V_d$) is very large. We are in the advection regime [2]: as soon as some liquid is withdrawn somewhere the particles do not have time to redistribute homogeneously in the liquid by diffusion because the characteristic diffusion velocity is smaller than the velocity of advancement of the front. The drying front velocity, equal to the drying rate expressed in the form of a velocity, i.e. $V = (1/\rho_0 S)\mathrm{d}m/\mathrm{d}t$ with $m$ the total sample mass, $\rho_0$ the liquid density and $S$ the sample cross-section, is larger than the characteristic diffusion velocity of a colloidal particle over the sample height ($H$) which expresses as $V_d = k_B T/\pi\mu RH$ in which $\mu$ is the liquid viscosity, $R$ the particle radius, $k_B$ the Boltzmann constant and $T$ the temperature. We have $V_d \approx 3.10^{-9}$ m.s$^{-1}$ while in our tests $V$ ranges from $10^{-6}$ m.s$^{-1}$ to $10^{-8}$ m.s$^{-1}$.

However, it is worth emphasizing that over a height of the order of 1 mm we have $V_d \approx V$, which means that within and below such a distance diffusion can play a significant role. Under these conditions the particle transport can be described by an advection-diffusion equation, leading in that case to an exponential increase of the concentration [14]. This explains the shape and thickness of the transition region in the particle concentration curve (see Figure 2b). Note that due to our poor resolution it does not appear relevant to attempt to check further the validity of this theory by fitting exponential curves to these data.

In order to understand how this distribution forms it is instructive to look at the evolution of the concentration of colloidal particles in the liquid phase. It appears that this concentration remains equal to the initial one in some (lower) region while it becomes equal to slightly more than 60% in an upper region of thickness growing in time (see Figure 2b). Such a concentration value is close to the maximum packing fraction of uniform spheres. Thus the process develops in the form of a *compacted front* progressing (receding) inside the sample. Note that in this region the pores are not saturated with a concentrated suspension, this is the remaining suspension volumes which are filled with colloidal particles (at the maximum packing fraction).

It is remarkable that in this compacted front the water saturation is very low whereas, below this region, it remains at a relatively high and almost uniform level which continuously decreases in time as the compacted front progresses (see Figure 2c). Such a horizontal profile over the whole sample and decreasing in time is usually observed when drying porous media saturated with a simple liquid [2, 3, 29, 30]. It is associated with a capillary re-equilibration process while the water evaporates essentially along the free surface of the sample. The origin of this effect is now well known: withdrawing water along the free surface creates menisci which induce a capillary depression (scaling as $\gamma/a$, with $\gamma$ the surface tension and $a$ the bead radius) tending to move upwards the liquid situated beneath via some global capillary re-equilibration process of the liquid network throughout the sample [15]. This process occurs as bursts [17] which allow for air penetration in the largest pores whatever their position in the sample. By this means the water moves towards the free surface in the liquid state. Since during this stage the whole sample remains wet the air inside the sample is saturated with vapour, which precludes any evaporation process. As a consequence the drying mainly results from evaporation along the liquid-air interfaces at the top of the sample, which are close to the ambient air in which the vapour density is generally much lower. This explains that the rate of drying remains almost constant as long as a capillary re-equilibration can occur, i.e. as long as the rate of evaporation is smaller than the rate of the flow in the liquid films induced by capillary effects. Since the latter phenomenon results from the liquid flow through a liquid network with channels of size proportional to $R$ under the action of the above capillary pressure the corresponding velocity ($V_f$) scales as $\beta\gamma R/\mu H$, in which $H$ is the sample height, and $\beta$ a coefficient related to the structure of the liquid network which is of the order of $0.002$ for a saturated bead packing [15]. Thus here $V_f$ is of the order of $10^{-5}$ m.s$^{-1}$, which is much larger than the drying velocity in our tests. This implies that in our case capillary re-equilibration is dominant in the wet region as long as the saturation is not too low.

In the compacted region there is still some water in the pores of this colloidal particle packing. However this water is trapped in nanopores (~3 nm) from which it does not easily escape. In particular its evaporation would lead to the exposure of the solid surface of colloid to air, which is not energetically favourable. This Kelvin effect suggests that the water in such pores may be at equilibrium with an external vapour density much smaller than 100% [31].

Moreover the liquid flow velocity under capillary pressure effect ($V_f$) is now of the order of $10^{-9}$ m.s$^{-1}$, much smaller than the drying velocity of our samples. We conclude that the liquid trapped in the compacted front then remained essentially static during the rest of the experiment; it negligibly takes part to the drying process of the rest of the sample. As a consequence it is likely that drying occurs via the evaporation from the upper surface of the uncompacted (wet) region then diffusion through some air network towards the free surface of the sample.

As a consequence the picture which emerges is as follows. The colloidal particles are transported with the liquid which is drained by capillary effects towards the free surface, where they store and start to form a compacted region. The drying then results from evaporation along the upper free surface of the wet region in the bead packing, i.e. just below the compacted front. This explains why the drying rate decreases and there is no constant rate period (see Figure 4). During this process the water in the wet region is still drained by capillary process towards the lower surface of the compacted front. Let us recall that although the particle concentration in the water volume is at its maximum value (around 60%) in the compacted region the volume fraction of suspension (water + particles) in the pores decreases downwards. Thus there is an air network starting from the free surface and with a corresponding concentration increasing downwards. This network allows for vapour diffusion from the upper surface of the wet region. The corresponding aspect of the material structure in time is represented schematically in Figure 3. In the bottom part, the saturation decreases and the colloidal concentration is low (close to the initial one); thus the volume fraction of colloids in the pore drops to zero, and the process removes the particles from the bottom.

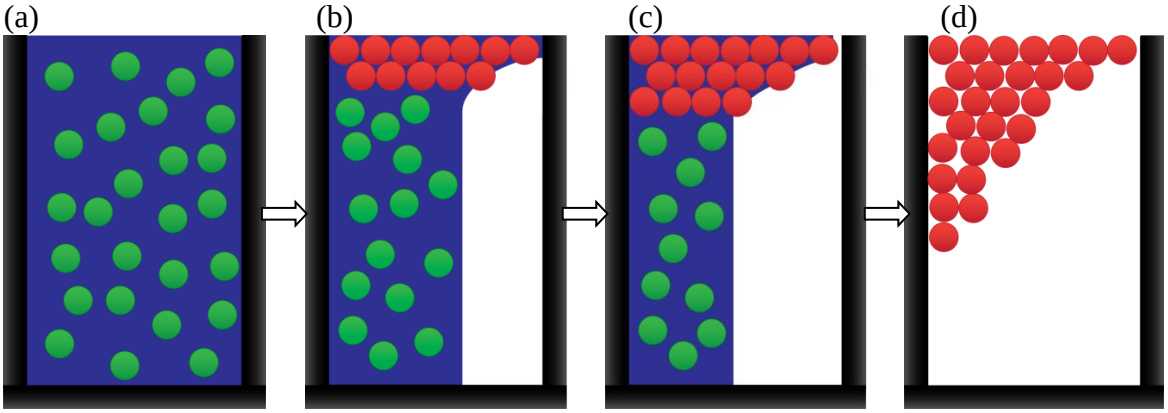


FIG.3. (Color online) Scheme of the drying mechanism in a porous media coupled with the transport of colloidal particles. The green particles are free to move in the liquid phase whereas the red ones are motionless in the compacted region. Initially (a) the particles are homogeneously dispersed in the medium and water saturation is at its maximum. Then the particles start to accumulate around the free surface of the sample (b). Afterwards the particles start forming a crust (c) and the saturation decreases in the whole sample. At the end of drying the compacted region extends throughout the sample but with an effective particle content decreasing downwards.

The fact that evaporation occurs from below the compacted region implies that the rate of drying will decrease all the faster as the compaction front grows more rapidly. This means that the rate of drying (expressed in relative value with regards to the initial water saturation) will decrease faster for a larger initial concentration of colloidal particles, while for a porous medium filled with pure water the rate of drying remains almost constant down to very low saturations. This shows that it is possible to control the rate of drying by adjusting the initial concentration of colloidal particles in the liquid (see Figure 4).

Our assumption about the main evaporation process taking place below the compacted region is confirmed by the fact that we can predict the rate of drying assuming diffusion over a distance equal to the measured thickness ( $z$ , see Figure 2.b.) of the compacted front. The rate of drying ( $J = \rho_0 V/\omega$ ) may be found from the diffusion equation [15] $J \approx D n_{sat}/(\delta + z)$, in which $D$ is the diffusion coefficient of water through the air ( $D_{water} = 2.7 10^{-5} \mathrm{m}^2.\mathrm{s}^{-1}$ ), $n_{sat}$ the maximum vapour density ( $n_{sat} = 23.4\,\mathrm{g.m}^{-3}$ ), and $\delta$ the initial equivalent diffusion length (related to the boundary layer thickness of the air flux, which varies from one test to another because it depends on the exact shape (roughness) of the top surface of the sample). Using the (measured) size ( $z$ ) of the compacted front in time (see Figure 2b) we computed the drying rate in time and thus the evolution of the water saturation. It appears that this model is in good agreement with the data which confirms the validity of our physical scheme, but some significant discrepancy is observed at concentrations larger than 15% (see dotted lines in Figure 4).

## 4. Modelling

We can now use all our knowledge of the process to develop a full modelling approach predicting the evolution of the rate of drying and the final distribution of particles without any measurement. As the particles act as markers of the fluid, due to the water arrival from below they accumulate and pack at $\psi_m \approx$ 60%, leading to an increase of the compacted region (of size $z$ ). The growth of this region is related to the drying rate via:

$$\psi_0 (1-\psi_0) J = \phi(\psi_m - \psi_0)\,\dot{z} \qquad (2)$$

Simultaneously, the bottom part of the sample (still liquid), which provides the evaporative water, desaturates homogenously so that the drying rate is also related to the saturation change in this region:

$$(1-\psi_0) J = -(H - z)\dot{\phi} \qquad (3)$$

Dropping $J$ from these two equations we get a differential equation which may be solved to find the relationship between the front advancement and the saturation. We can in particular deduce the final distribution of particles as a function of the depth $z$, i.e. $\chi_{final}(z) = \psi_m/\left(1-\psi_m\right)\phi(z)\big)$. This gives:

$$\chi_{final}(z) = \psi_m \left(1 - z/H\right)^{(\psi_m - \psi_0)/\psi_0} \qquad (4)$$

It is worth noting that this distribution (shown in Figure 2a) is independent of the drying history. From this model we can also compute a characteristic length λ, over which the final volume fraction is significant with regards to the initial volume fraction of particles. Assuming this situation is reached when the particle fraction is negligible in the rest of the sample, say when $\chi_{final}(\lambda) \approx \psi_0/10$, we get $\lambda = H\left(1-\left(\psi_0/(10\psi_m)\right)^{\psi_0/(\psi_m-\psi_0)}\right)$. For $\psi_0 = 5\%$ we find $\lambda = 1.4\,\mathrm{cm}$, which means that all the particles are essentially in the first 1.4 cm, leaving particle-free the bottom of the sample.

Now using the expression for the drying rate due to diffusion as a function of the depth of the compaction front we can solve numerically these coupled differential equations to predict the drying rate in time. The computed mass of water, integrated from the drying rate, appears to be in excellent agreement with the measures from MRI (see continuous lines in Figure 4).

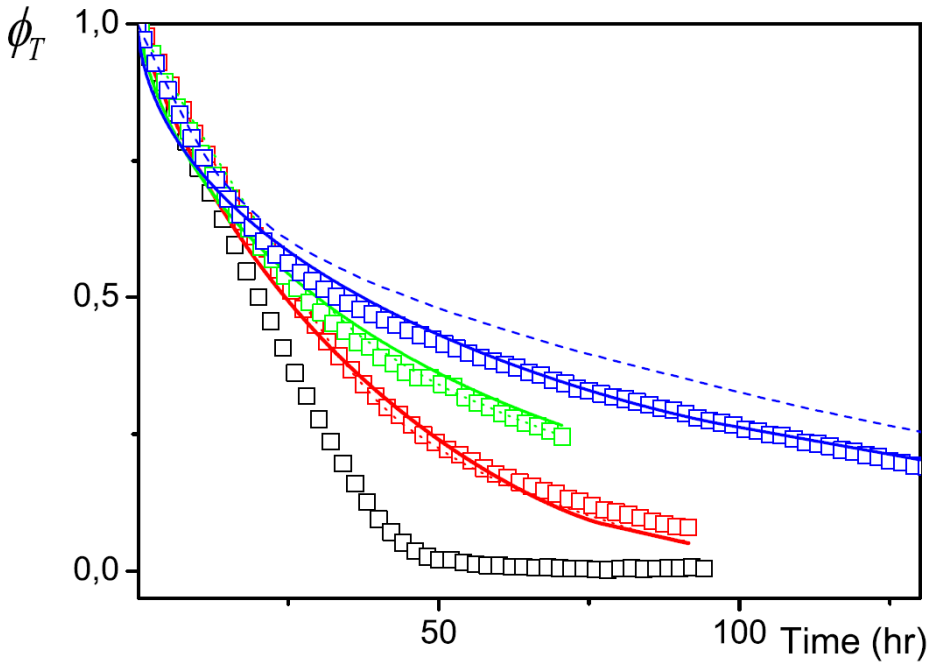


FIG. 4. (Color online) Total water saturation (ratio of the total mass of water to the initial mass of water) as a function of time during the drying of a porous medium. Initially filled with: (black, bottom) pure water, (red, dark gray) 5% colloidal particles in water, (green, light gray) 10%, (blue, upper) 15%. The square symbols correspond to the experimental data. The dotted lines correspond to the modelling approach based on the measure of the compacted front thickness, and the continuous lines to the full modelling approach.

## 5. Conclusion

Using a new $^1$H MRI protocol to observe nanoparticles in an unsatured porous medium, we show that colloidal particles move towards the free surface, an effect that create a surprising heterogeneity in the solid. Since our measurements provided a detailed understanding of the physical mechanism at work we propose a simple model based on advection which predicts quite well both the distribution of particles in time and the drying rate. This suggests a

technique for controlling the drying rate of porous media, by introducing an appropriate volume fraction of colloidal particle in the liquid. An important next step would be to take into account the possible interactions between colloidal particles or their adsorption on pore walls.

**Acknowledgments**: We are grateful to David Hautemayou for his technical support.

## References

1. R. Helmig, Multiphase Flow and Transport Processes in the Subsurface (Springer, Berlin, 1997) – E. Michel, S. Majdalani and L. Di-Pietro, Vadose Zone Journal 9, 307 (2010).
2. Y. Puyate, C. Lawrence, N. Buenfeld and I. McLoughlin, Physics of Fluids, 10, 566, (1998) – L. Pel, H. Huinink, K. Kopinga, R. v. Hees and O. Adan, Construction and Building Materials 18, 309 (2004).
3. C. Gauthier, D. Nadji and P. Coussot, C. R. Acad. Sci. Paris 326, 767 (1998).
4. B. Alramahi, K. Alshibli and D. Fratta, J. of geotechnical and geoenvironmental 136, 620 (2010) – A. Vendelboe, P. Moldrup, P. Schjonning, D. Oyedele, Y. Jin, K. Scow and L. de Jonge, Vadose Zone Journal 11, 0070 (2012).
5. R. D. Deegan, O. Bakajin, T.F. Dupont, G. Huber, S.R. Nagel, T.A. Witten, Nature (London) 389, 827 (1997).
6. J. Li, B. Cabane, M. Sztucki, J. Gummel and L. Goehring, Langmuir 28, 200 (2012)
7. N. Shokri, P. Lehmann, D. Or, Geophys. Res. Lett., 35, L19407 (2008)
8. H. Hu and R.G. Larson, J. Phys. Chem. B 106, 1334 (2002).
9. P. J. Yunker, T.Still, M. A. Lohr and A. G. Yodh, Nature (London) 476, 308 (2011).
10. A. G. Marín, H. Gelderblom, D. Lohse and J. H. Snoeijer, Phys. Rev. Lett. 107, 085502 (2011).
11. L. Pauchard and C. Allain, Europhys. Lett. 62, 897 (2003).
12. E.R. Dufresne, E. I. Corwin, N.A. Greenblatt, J. Ashmore, D.Y.Wang, A.D. Dinsmore, J.X. Cheng, X. S. Xie, J.W. Hutchinson, and D.A.Weitz, Phys. Rev. Lett. 91, 224501 (2003).
13. N. Tsapis, E. R. Dufresne, S. S. Sinha, C. S. Riera, J.W. Hutchinson, L. Mahadevan, and D. A. Weitz, Phys. Rev. Lett. 94, 018302 (2005).
14. A. Merlin, J.-B. Salmon and J. Leng, Soft Matter 8, 3526 (2012)
15. P. Coussot, Eur. Phys. J. B 15, 557 (2000).
16. A. G. Yiotis, A. G. Boudouvis, A. K. Stubos, I. N. Tsimpanogiannis, and Y. C. Yortsos, Phys. Rev. E 68, 037303 (2003)
17. L. Xu, S. Davies, A.B. Schofield and D.A. Weitz, Phys. Rev. Lett. 101, 094502 (2008).
18. N. Shahidzadeh-Bonn, A. Tournie, S. Bichon et al., Transport in Porous Media 56, 209, (2004)
19. P. J. McDonald, J.-P. Korb, J. Mitchell and L. Monteilhet, Phys. Rev. E 72, 011409 (2005) J. M. Salamanca et al., Langmuir 17, 3202 (2001) – T. Mizuguchi, A. Nishimoto, S.
20. Kitsunezaki, Y. Yamazaki, I. Aoki, Phys. Rev. E 71, 056122 (2005) – R. E. Trueman, E. Lago Domingues, S. N. Emmett, M. W. Murray, J. L. Keddie and A. F. Routh, Langmuir 28, 3420 (2012)
21. H. Carr and E. Purcell, Physical Review 94, 630 (1954).
22. S. Meiboom and D. Gill, Review of Scientific Instruments 29, 688 (1958).
23. K. Brownstein and C. Tarr, Phys. Rev. A 19, 2446 (1979).

24. K. Brownstein and C. Tarr, J. of Magnetic Resonance 26, 17 (1977).
25. S.V. Dvinskikh, K. Szutkowski, I. Furó, J. of Magnetic Resonance 198 ,146 (2009)
26. P. F. Faure and S. Rodts, Magnetic Resonance Imaging 26, 1183 (2008)
27. J.-P. Korb, Current Opinion in Colloid and Interface Science 14, 192 (2009)
28. S. Rodts et al, Phys. Rev. E 81, 021402 (2010)
29. N. Shahidzadeh-Bonn, A. Azouni and P. Coussot, J. Phys.: Condens. Matter 19, 112101 (2007).
30. P. Faure and P. Coussot, Phys. Rev. E 82, 036303 (2010).
31. O. Coussy, Poromechanics (J. Wiley & Sons, Chichester, 2004).